Thermal rectification and spin-spin coupling of nonreciprocal localized and surface modes

Annika Ott and Svend-Age Biehs*
Institut für Physik, Carl von Ossietzky Universität, D-26111 Oldenburg, Germany

(Received 17 February 2020; revised manuscript received 5 April 2020; accepted 6 April 2020; published 24 April 2020)

We study the rectification of near-field radiative heat transfer between two InSb nanoparticles due to the presence of nonreciprocal surface modes in a nearby InSb sample when an external magnetic field is applied and its dependence on the magnetic field strength. We reveal the spin-spin coupling mechanism of the localized particle resonances and the surface mode resonances which is substantiated by the directional heat flux in the given setup. We discuss further the interplay of the frequency shift, the propagation length, and local density of states on the strength and directionality of the rectification as well as the nonreciprocal heating effect of the nanoparticles.

DOI: 10.1103/PhysRevB.101.155428

I. INTRODUCTION

In the last few years, it could be shown that the nonreciprocal behavior of magneto-optical materials like InSb has very interesting consequences for nanoscale thermal radiation. For example, fundamental effects like a persistent heat current [1,2], giant magnetoresistance [3,4], thermal Hall effect [5], as well as a circular heat flux, angular momentum, and spin which do also persist in global equilibrium [6] were highlighted. As reviewed and discussed in detail in Ref. [7] magneto-optical materials and in particular these fundamental effects might have applications in the control of magnitude [8–10] and direction of radiative heat fluxes in nanoscale systems. Furthermore, it could be shown that nonreciprocal materials can also be utilized to introduce a near-field heat flux rectification. So far, most of the concepts for thermal rectification are based on the temperature dependence of the material properties [11–16] which can be very strong for phase-change materials like VO_2 [17], which show up to date the strongest diode effect for thermal radiation [18–21]. Recently, it has been demonstrated that a thermal emitter and receiver can show an enhanced heat exchange by transporting the heat via the surface modes of a third body in their close vicinity [22–30] or by coupling to large wave-vector propagating modes in hyperbolic materials which is very similar to the Förster resonance energy transfer enhancement observed in plasmonic and hyperolic environments [31–34]. This coupling effect opens up a new possibility to rectify the radiative heat flux between a thermal emitter and receiver by introducing surfaces supporting nonreciprocal surface modes [35–37]. As has been shown by us, nonreciprocal surface modes allow to rectify the radiative heat flux very efficiently [38].

In this work, we will discuss our diode concept [38] as depicted in Fig. 1 in much greater detail. In this configuration, two InSb nanoparticles are held in close vicinity to an InSb substrate. The nanoparticles can exchange heat via direct coupling or coupling to the surface modes. To quantify this heat exchange, we first derive the many-body expressions for the power exchanged between N nanoparticles in a given in general nonreciprocal environment as well as the many-body expression of the mean Poynting vector and discuss these quantities for the special case of $N = 2$. We will show that the coupling to the surface modes is dictated by a spin-spin coupling mechanism which is behind the diode effect. We substantiate our interpretation by discussing the impact of the surface mode splitting, the propagation length, local density of states and the heat flux in the three-body structure as well as the thermal relaxation into the nonequilibrium steady state (NESS). We find, that the nonreciprocal heating of the nanoparticles can be on the order of 15% of the applied temperature difference.

II. HEAT FLUX

In order to investigate heat flux rectification we consider the system shown in Fig. 1. Two identical spherical nanoparticles 1 and 2 with radius R and interparticle distance d are placed in plane parallel to a substrate at a distance z. We will assume that the particles are so small that we can describe them as dipoles with a polarizability $\underline{\alpha}$. This assumption is valid for particles much smaller than the dominant thermal wavelength which is about 10 μm in our case and if the distances d between the particles and z between the particles and the substrate are at least $4R$ [39–41]. The particles and the substrate are made of a magneto-optical material supporting localized and surface resonances in the spectral window important for heat exchange at temperatures around 300 K. In this work we chose InSb for the particles and for the substrate. Moreover, the background is vacuum. We assume throughout the work that the particles and their environment or background (substrate and vacuum background) can be assumed to be in local thermal equilibrium at temperatures T_1, T_2, and T_b. This assumption is valid as long as the radiative heat flux is less important than the heat conduction inside the materials, which is definitely fulfilled in our configuration.

*s.age.biehs@uni-oldenburg.de

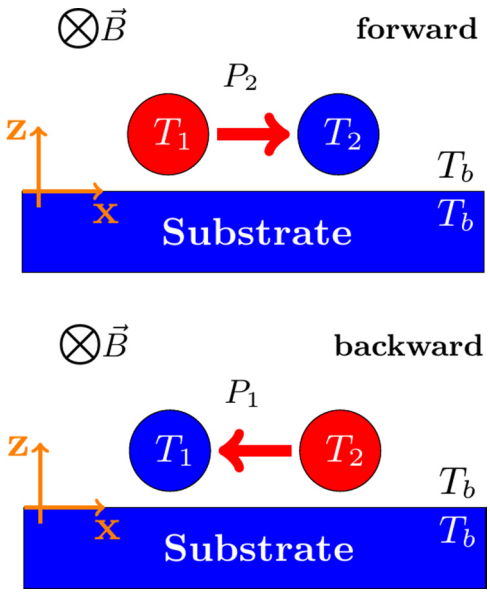

FIG. 1. Sketch of the considered system. Two InSb particles are in vicinity of an InSb substrate at a distance z. (Top) Particle 1 is heated with respect to particle 2 and the background, i.e., the temperature $T_1 > T_2 = T_b$. (Bottom) Reversed situation. Particle 2 is heated with respect to particle 1 and the background $T_2 > T_1 = T_b$.

Furthermore, the assumption is only valid on timescales which are much larger than the timescale of thermal relaxation of the materials. This is again true since the heat conduction inside the materials is much larger than the heat conduction by thermal radiation between the particles and between the particles and the substrate.

We can now determine the heat flux transferred between the two particles by calculating the net mean power $\langle P_i \rangle$ received by the ith particle. We start here with the more general case that there are N identical particles over a substrate following the derivations given in Ref. [42] and set $N = 2$ at the end. The total electric field $\vec{E}_i$ at the position of the ith particle is given by the field contributions due to the fluctuating dipole moments $\vec{p}_j^{\,\mathrm{fl}}$ of all particles $j \neq i$ and the background field $\vec{E}_i^{\,b}$ including direct thermal emission and multiple scattering. It can be written as [42]

$$\begin{pmatrix} \vec{E}_1 \\ \vdots \\ \vec{E}_N \end{pmatrix} = \boldsymbol{D}\boldsymbol{T}^{-1} \begin{pmatrix} \vec{p}_1^{\,\mathrm{fl}} \\ \vdots \\ \vec{p}_N^{\,\mathrm{fl}} \end{pmatrix} + (\mathbf{1} + \boldsymbol{D}\boldsymbol{T}^{-1}\boldsymbol{A}) \begin{pmatrix} \vec{E}_1^{\,b} \\ \vdots \\ \vec{E}_N^{\,b} \end{pmatrix}. \tag{1}$$

Similarly the induced dipole moments $\vec{p}_i$ for each particle i can be expressed in term of the fluctuating dipole moments of all other particles and the background field [42]

$$\begin{pmatrix} \vec{p}_1 \\ \vdots \\ \vec{p}_N \end{pmatrix} = \boldsymbol{T}^{-1} \begin{pmatrix} \vec{p}_1^{\,\mathrm{fl}} \\ \vdots \\ \vec{p}_N^{\,\mathrm{fl}} \end{pmatrix} + (\boldsymbol{T}^{-1}\boldsymbol{A}) \begin{pmatrix} \vec{E}_1^{\,b} \\ \vdots \\ \vec{E}_N^{\,b} \end{pmatrix}. \tag{2}$$

Here we have used the auxilliary $3N \times 3N$-block matrices [42]

$$\mathbf{1}_{ij} = \delta_{ij}\mathbb{1}, \tag{3}$$

$$\boldsymbol{T}_{ij} = \delta_{ij}\mathbb{1} - (1-\delta_{ij})k_0^2 \underline{\underline{\alpha}}\mathbb{G}_{ij}, \tag{4}$$

$$\boldsymbol{D}_{ij} = \epsilon_0\mu_0\mathbb{G}_{ij}, \tag{5}$$

and

$$\boldsymbol{A}_{ij} = \epsilon_0\delta_{ij}\underline{\underline{\alpha}} \tag{6}$$

with the Green functions $\mathbb{G}_{ij} = \mathbb{G}^{\mathrm{EE}}(\vec{r}_i, \vec{r}_j)$ for the electric field due to electric sources as defined in Ref. [43] and explicitely given in Appendix A.

With these expressions the net mean power received by particle i defined as [42]

$$\begin{aligned} \langle P_i \rangle &= \left\langle \frac{d\vec{p}_i(t)}{dt} \cdot \vec{E}_i(t) \right\rangle \\ &= 2\mathrm{Im} \int_0^\infty \frac{d\omega}{2\pi} \langle \vec{p}_i(\omega) \cdot \vec{E}_i^*(\omega) \rangle \end{aligned} \tag{7}$$

can be determined by inserting the above expressions. In order to evaluate the ensemble averages $\langle \circ \rangle$, we assume local thermal equilibrium of the background field and the particles so that we can exploit the fluctuation-dissipation theorem for the fields [42]

$$\langle \vec{E}_i^{\,b} \otimes \vec{E}_j^{\,b^*} \rangle = 2\omega^2\mu_0\hbar\left(n_b + \frac{1}{2}\right)\frac{\mathbb{G}_{ij} - \mathbb{G}_{ji}^\dagger}{2\mathrm{i}} \tag{8}$$

and for the fluctuating dipole moments [42]

$$\langle \vec{p}_i^{\,\mathrm{fl}} \otimes \vec{p}_j^{\,\mathrm{fl}*} \rangle = 2\epsilon_0\hbar\delta_{ij}\left(n_i + \frac{1}{2}\right)\underline{\underline{\chi}}. \tag{9}$$

Here we have introduced the mean occupation number $n_{i/b} \equiv n(T_{i/b}) = 1/(\exp(\hbar\omega/k_\mathrm{B}T_{i/b}) - 1)$ with the reduced Planck constant $\hbar$ and Boltzmann constant k_B. With these definitions and relations we finally obtain

$$\begin{aligned} \langle P_i \rangle = 4\mathrm{Im} \int_0^\infty \frac{d\omega}{2\pi} \hbar\omega \sum_{j=1}^{N} (n_j - n_b) \\ \times \mathrm{Tr}\left[\boldsymbol{T}_{ij}^{-1} \underline{\underline{\chi}}_j (\boldsymbol{D}\boldsymbol{T}^{-1})_{ij}^\dagger \right] \end{aligned} \tag{10}$$

with the generalized suszeptibility

$$\underline{\underline{\chi}}_i = \frac{\underline{\underline{\alpha}} - \underline{\underline{\alpha}}^\dagger}{2\mathrm{i}} - k_0^2 \underline{\underline{\alpha}} \cdot \frac{\mathbb{G}_{ii} - \mathbb{G}_{ii}^\dagger}{2\mathrm{i}} \cdot \underline{\underline{\alpha}}^\dagger \tag{11}$$

of the ith particle.

In our special case of two particles which are in a plane parallel to the substrate, we have $\underline{\underline{\chi}}_1 = \underline{\underline{\chi}}_2$ because $\mathbb{G}_{11} = \mathbb{G}_{22}$ due to translational symmetry. Furthermore, for $N = 2$, the mean power received by particle 1 is

$$\langle P_1 \rangle = 3 \int_0^\infty \frac{d\omega}{2\pi} \hbar\omega \left[(n_1 - n_b)\mathcal{T}_1^a + (n_2 - n_b)\mathcal{T}_1^b \right] \tag{12}$$

introducing the transmission coefficients

$$\mathcal{T}_1^a = \frac{4k_0^2}{3}\mathrm{Im}\mathrm{Tr}\big[\mathbb{D}_{121}^{-1}\underline{\underline{\chi}}_1 \times \left(\mathbb{G}_{11}\mathbb{D}_{121}^{-1} + \mathbb{G}_{12}\mathbb{D}_{212}^{-1}k_0^2\underline{\underline{\alpha}}\mathbb{G}_{21}\right)^\dagger\big], \tag{13}$$

$$\mathcal{T}_1^b = \frac{4k_0^2}{3}\mathrm{Im}\mathrm{Tr}\big[\mathbb{D}_{121}^{-1}k_0^2\underline{\underline{\alpha}}\mathbb{G}_{12}\underline{\underline{\chi}}_2 \times \left(\mathbb{G}_{11}\mathbb{D}_{121}^{-1}k_0^2\underline{\underline{\alpha}}\mathbb{G}_{12} + \mathbb{G}_{12}\mathbb{D}_{212}^{-1}\right)^\dagger\big] \tag{14}$$

with the wave number in vacuum $k_0 = \omega/c$, where c is the vacuum light velocity.

$$\mathbb{D}_{iji} := \mathbb{1} - k_0^4\underline{\underline{\alpha}}\mathbb{G}_{ij}\underline{\underline{\alpha}}\mathbb{G}_{ji}. \tag{15}$$

The expression for $\langle P_2\rangle$ can be obtained by interchanging $1 \leftrightarrow 2$. In the backward case with $T_1 = T_b$ and $T_2 > T_1$, i.e., when particle 2 is heated with respect to its environment (see Fig. 1), then the power $\langle P_1\rangle$ received by particle 1 describes the heat flux from particle 2 to particle 1 which is obviously described by the transmission coefficient $\mathcal{T}_1^b$. Similarly $\mathcal{T}_2^b$ would describe the heat flux from particle 1 to particle 2 in the forward case where $T_2 = T_b$ and $T_1 > T_2$ (see Fig. 1). As shown explicitely in Ref. [44], for reciprocal particles and substrate, i.e., if $\underline{\underline{\alpha}}^t = \underline{\underline{\alpha}}$ and $\mathbb{G}_{ij} = \mathbb{G}_{ji}^t$, we find $\mathcal{T}_1^b = \mathcal{T}_2^b$. The heat flux in forward and backward direction is the same. Now, if the particles or the environment are nonreciprocal then $\mathcal{T}_1^b \neq \mathcal{T}_2^b$ in general [44]. Hence, for nonreciprocal materials the heat flux in forward and backward direction are not the same. In the following, we will show that when applying a magnetic field the nonreciprocal surface modes in the InSb sample will result in a large heat flux rectification.

III. MATERIAL PROPERTIES

For an applied magnetic field in positive y direction, the permittivity of InSb is given by

$$\underline{\underline{\epsilon}} = \begin{pmatrix} \epsilon_1 & 0 & \mathrm{i}\epsilon_2 \\ 0 & \epsilon_3 & 0 \\ -\mathrm{i}\epsilon_2 & 0 & \epsilon_1 \end{pmatrix} \tag{16}$$

with [46]

$$\frac{\epsilon_1}{\epsilon_\infty} = \left(1 + \frac{\omega_\mathrm{L}^2 - \omega_\mathrm{T}^2}{\omega_\mathrm{T}^2 - \omega^2 - \mathrm{i}\Gamma\omega} + \frac{\omega_\mathrm{p}^2(\omega + \mathrm{i}\gamma)}{\omega[\omega_\mathrm{c}^2 - (\omega + \mathrm{i}\gamma)^2]}\right), \tag{17}$$

$$\frac{\epsilon_3}{\epsilon_\infty} = \left(1 + \frac{\omega_\mathrm{L}^2 - \omega_\mathrm{T}^2}{\omega_\mathrm{T}^2 - \omega^2 - \mathrm{i}\Gamma\omega} - \frac{\omega_\mathrm{p}^2}{\omega(\omega + \mathrm{i}\gamma)}\right), \tag{18}$$

and

$$\frac{\epsilon_2}{\epsilon_\infty} = \frac{\omega_\mathrm{p}^2\omega_\mathrm{c}}{\omega[(\omega + \mathrm{i}\gamma)^2 - \omega_\mathrm{c}^2]} \tag{19}$$

with the cyclotron frequency $\omega_c = eB/m^*$, the effective mass $m^* = 7.29 \times 10^{-32}$ kg, the density of the free charge carriers $n = 1.36 \times 10^{19}$ cm^{-3} [45], the dielectric constant for infinite frequencies $\epsilon_\infty = 15.68$, the longitudinal and transversal optical phonon frequency $\omega_\mathrm{L} = 3.62 \times 10^{13}$ rad/s and $\omega_\mathrm{T} = 3.39 \times 10^{13}$ rad/s [46]. With these parameters, the plasma frequency of the free carriers is $\omega_\mathrm{p} = \sqrt{\frac{ne^2}{m^*\epsilon_0\epsilon_\infty}} = 1.86 \times 10^{14}$ rad/s. Furthermore, we use the phonon damping constant $\Gamma = 5.65 \times 10^{11}$ rad/s and the free charge carrier damping constant $\gamma = 10^{12}$ rad/s [45].

From the above expressions for the permittivity it can be seen that the permittivity tensor is diagonal, if no magnetic field is applied ($B = 0$) and therefore $\underline{\underline{\epsilon}} = \underline{\underline{\epsilon}}^t$. On the other hand, if $B \neq 0$ the permittivity is nonreciprocal, i.e., $\underline{\underline{\epsilon}} \neq \underline{\underline{\epsilon}}^t$, due to the Lorentz force acting on the electrons inside InSb. This will have an impact not only on the surface modes in the InSb sample but also on the localized resonances of the InSb nanoparticles.

IV. LOCALIZED MAGNETO-OPTICAL PLASMONS OF THE NANOPARTICLES

In dipole approximation, the polarizability of the particles is [47]

$$\underline{\underline{\alpha}} = 4\pi R^3(\underline{\underline{\epsilon}} - \mathbb{1})(\underline{\underline{\epsilon}} + 2\mathbb{1})^{-1}. \tag{20}$$

Thus, due to the nonreciprocity of the permittivity, the polarizability becomes nonreciprocal as well, i.e., when a magnetic field is applied we have $\underline{\underline{\alpha}} \neq \underline{\underline{\alpha}}^t$. Furthermore, as discussed in detail in Ref. [6] the threefold degenerate localized dipolar resonances at $\omega_{m=0,\pm1}$ determined by the poles of $\underline{\underline{\alpha}}$ with magnetic quantum numbers $m = 0, \pm1$ split into three nondegenerated resonances where the splitting of the resonances with $m = \pm1$ is mainly given by the cyclotron frequency ω_c. As shown in Ref. [6], these resonances are connected with a clockwise or counter-clockwise radiative heat flux for $m = -1$ or $m = +1$ as well as an angular momentum and spin which also persist in global thermal equilibrium and which are at the heart of the persistent heat current and thermal Hall effect in many-particle assemblies [1,5–7]. As shown in Ref. [6] the mean spin for $m = -1$ ($m = +1$) is parallel (antiparallel) to the magnetic field resulting in a blue (red) shift so that the splitting can be understood as an analog of the Zeeman splitting.

V. MAGNETO-OPTICAL SURFACE MODES OF THE SUBSTRATE

The nonreciprocity introduced by the magnetic field also affects the surface modes of the InSb sample [35–37]. To see this effect and to determine the heat transfer, we have determined the reflection matrix which has in the polarization basis of s and p polarization (TE and TM modes) the form

$$\mathbb{R} = \begin{pmatrix} r_{ss} & r_{ps} \\ r_{sp} & r_{pp} \end{pmatrix} \tag{21}$$

analogously to the approach in Ref. [48] by solving the Booker equation analytically. For $B = 0$ the nondiagonal elements r_{sp} and r_{ps} describing depolarization effects vanish. But even for $B \neq 0$ they turn out to be small compared to r_{ss} and r_{pp} for the parameters used in our work. Therefore the reflection coefficients r_{sp} and r_{ps} can be neglected. Furthermore, to study the impact of the magnetic field on the surface modes it suffices to focus on r_{pp}. Considering the Voigt configuration as depicted in Fig. 1 where the magnetic field is in y direction and the surface modes travel in $\pm k_x$ direction, the reflection

coefficient can be written as

$$r_{pp} = \frac{\left(k_0^2 - k_z k_z^-\right)\left(k_x^2 - k_0^2\epsilon_1\right) + k_z k_x\left(k_0^2 \mathrm{i}\epsilon_2 + k_x k_z^-\right)}{k_z k_x\left(k_0^2 \mathrm{i}\epsilon_2 + k_x k_z^-\right) - \left(k_0^2 - k_z k_z^-\right)\left(k_x^2 - k_0^2\epsilon_1\right)} \tag{22}$$

introducing the wave vector components

$$k_z = \sqrt{k_0^2 - k_x^2}, \tag{23}$$

$$k_z^- = \sqrt{k_0^2\epsilon_v - k_x^2} \tag{24}$$

with the Voigt permittivity

$$\epsilon_v = \frac{\epsilon_1^2 - \epsilon_2^2}{\epsilon_1}. \tag{25}$$

Now, the dispersion relation of the surface modes is given by the poles of r_{pp}. We obtain

$$k_x^2 - k_0^2\epsilon_1 - k_z k_z^- \epsilon_1 - k_z k_x \mathrm{i}\epsilon_2 = 0 \tag{26}$$

which is the same expression as in Ref. [37]. It can already be seen that this dispersion relation depends on the sign of k_x. Hence, surface modes propagating to positive or negative x direction have in general different dispersion relations if $\epsilon_2 \neq 0$, i.e., if a magnetic field is applied. Furthermore, in the quasistatic regime $k_x^2 \gg k_0^2, k_0^2|\epsilon_v|$, we retrieve the result [37] $\epsilon_1 + \epsilon_2 = -1$ for $k_x > 0$ and $\epsilon_1 - \epsilon_2 = -1$ for $k_x < 0$ reflecting again the fact that the surface modes propagating in positive or negative x direction are differently affected by the magnetic field which introduces this nonreciprocity. This nonreciprocity is more generally expressed by that fact that $r_{pp}(k_x) \neq r_{pp}(-k_x)$ when a magnetic field is applied in y direction. As a consequence also the Green tensor becomes nonreciprocal in this case and of course it is clear that the heat flux from particle 1 to particle 2 due to the coupling to the surface waves will be different from the heat flux from particle 2 to particle 1.

The nonreciprocal behavior of the surface modes can be seen in Fig. 2 where we have plotted $1 - |r_{pp}|^2$ for the propagating waves with $k_x^2 \leqslant k_0^2$ and $\mathrm{Im}(r_{pp})$ for the evanescent waves with $k_x^2 > k_0^2$. These quantities reflect the absorbed energy by reflection of incident propagating and evanescent waves. We have also plotted the dispersion relation of the surface modes in Eq. (26). It can be easily seen that the symmetry of r_{pp} with respect to k_x is broken when a magnetic field $B \neq 0$ is applied in y direction. A splitting of the two resonances can be seen, where the surface modes traveling in positive x direction are redshifted whereas the surface modes traveling in negative x direction are blueshifted [35]. As discussed in Ref. [49,50] there is a spin momentum locking of the surface waves. The surface waves for $k_x < 0$ have a spin in positive y direction, i.e., in the direction of the magnetic field, whereas the surface waves for $k_x > 0$ have a spin in negative y direction, i.e., opposite to the magnetic field. From this one, can intuitively understand the redshift of the resonance frequency for surface waves with $k_x > 0$ and the blue shift for surface waves with $k_x < 0$ which is again simply analogous to the Zeeman effect.

VI. LOCAL DENSITY OF STATES

The fact, that the presence of the magnetic field introduces a nonreciprocity or asymmetry for the waves propagating

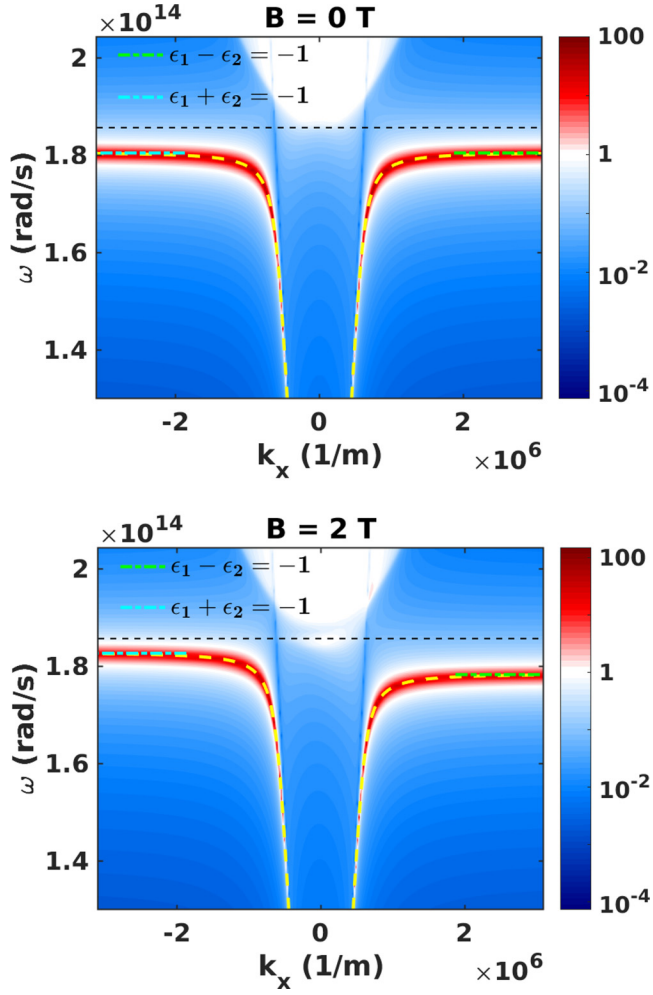

FIG. 2. Parallel part of the reflection coefficient r_{pp} for the Voigt configuration in ω-k_x plane with $k_y = 0$ and $B = 0$ (top) and 2 T (bottom). For propagating waves with $k_x^2 \leqslant k_0^2$ the quantitiy $1 - |r_{pp}|^2$ is shown and for evanescent waves with $k_x^2 > k_0^2$ the quantity $\mathrm{Im}(r_{pp})$ is plotted. The yellow dashed line is the dispersion relation in Eq. (26). The dashed green and blue curves show the quasistatic limit of the dispersion relation. The horizontal dashed line marks the plasma frequency of InSb.

in positive or negative x direction motivates to divide the expression for the local density of states (LDOS) $D(\omega, z)$ into two parts $D^{\pm}(\omega, z)$ belonging to exactly such waves with $k_x > 0$ and $k_x < 0$. Thus we define $D^{\pm}(\omega, z)$ by starting from the well-known expression of the LDOS at a distance z above a semi-infinite medium [51]

$$D(\omega, z) = \int_{-\infty}^{\infty} \frac{dk_x}{2\pi} \int_{-\infty}^{\infty} \frac{dk_y}{2\pi} f(\kappa, \omega, z) \tag{27}$$

with $\kappa^2 = k_x^2 + k_y^2$ and

$$f(\kappa, \omega, z) = \frac{\omega}{\pi c^2} \mathrm{Im} \frac{\mathrm{i}}{2\sqrt{k_0^2 - \kappa^2}} \times \left[4 + \frac{2\kappa^2}{k_0^2}\left((r_{ss} + r_{pp}) e^{2\mathrm{i}\sqrt{k_0^2 - \kappa^2} z}\right)\right]. \tag{28}$$

Strictly speaking this expression is only valid for media with $r_{sp} = r_{ps} = 0$. Since, we find for InSb with our choice of

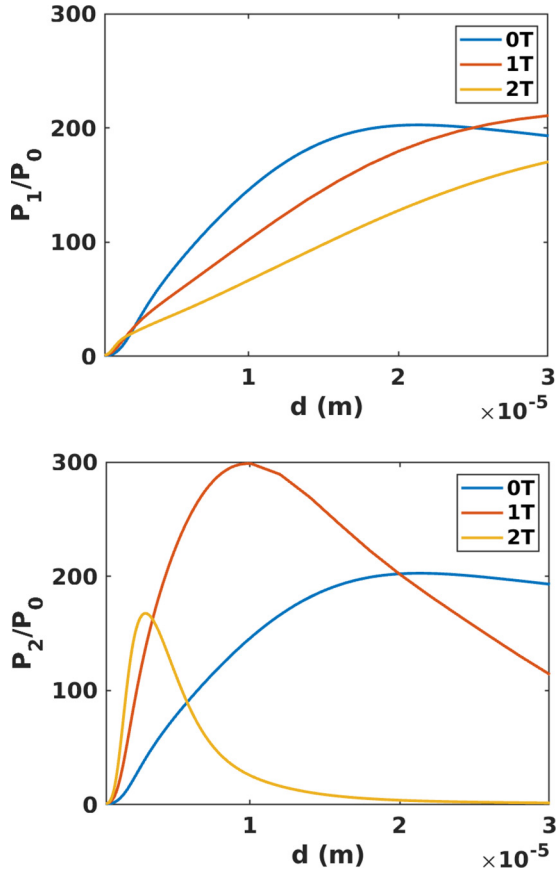

FIG. 3. Net transferred power P_1 and P_2 on the colder particles in the backward and forward case (see Fig. 1) as function of interparticle distance d for different strengths of the magnetic field $B = 0,\ 1,$ and 2 T. The distance to the substrate is $z = 5R = 500$ nm. The transferred power is normalized to the value P_0 where the substrate is replaced by vacuum.

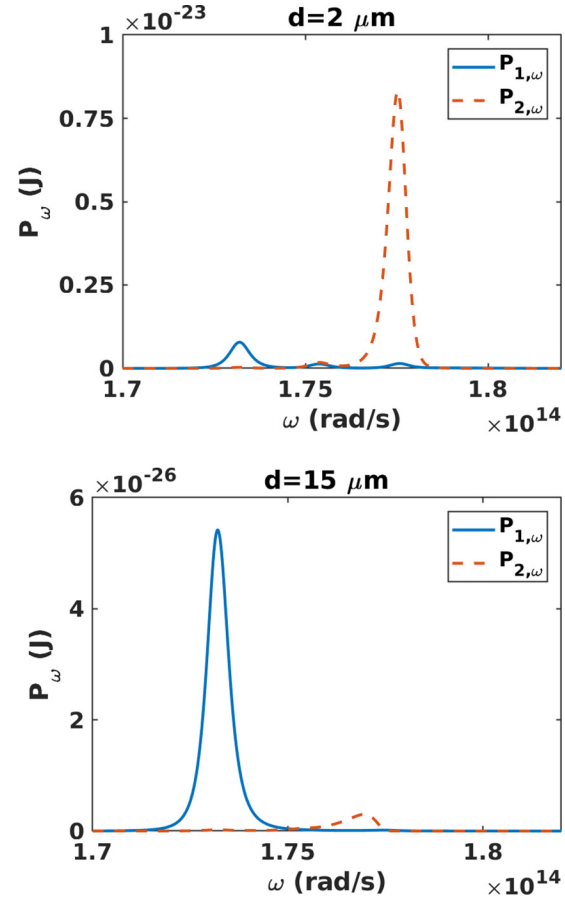

FIG. 4. Spectral net power in forward and backward direction for $d = 2$ and 15 μm and $B = 2$ T. The distance to the substrate is $z = 5R = 500$ nm.

parameters that these depolarization components are negligible small compared to r_{ss} and r_{pp}, we can also use this expression of the LDOS to characterize our InSb sample. Now, we define $D^{\pm}(\omega, z)$ by considering only the contributions for the waves traveling in positive and negative x direction

$$D^{+}(\omega, z) = \int_0^{\infty} \frac{dk_x}{2\pi} \int_{-\infty}^{\infty} \frac{dk_y}{2\pi} f(\kappa, \omega, z), \tag{29}$$

$$D^{-}(\omega, z) = \int_{-\infty}^{0} \frac{dk_x}{2\pi} \int_{-\infty}^{\infty} \frac{dk_y}{2\pi} f(\kappa, \omega, z). \tag{30}$$

In Fig. 6, we will use this quantity to discuss the heat flux rectification.

VII. HEAT TRANSFER MECHANISM

Due to the nonreciprocal behavior of the surface modes the heat fluxes between the two particles can become asymmetric if the heat flux is dominated by the contribution of the surface modes. To study this effect, we consider now the configuration shown in Fig. 1 for the backward scenario with $T_1 = T_b = 300$ K and $T_2 = 350$K and the forward scenario with $T_2 = T_b = 300$ K and $T_1 = 350$ K chosing $z = 5R = 500$ nm. In Fig. 3, the net power $P_1 \equiv \langle P_1 \rangle$ received by particle 1 in the backward case and the net power $P_2 \equiv \langle P_2 \rangle$ received by particle 2 in the forward case are shown for different interparticle distances d. Note that these powers are normalized to the value P_0 where the substrate is replaced by vacuum. It can be easily seen that $P_1 \neq P_2$ if $B \neq 0$ and that the maximum of P_1/P_0 at position d_m moves to larger distances d out of the plotted region when increasing the magnetic field amplitude, whereas the maximum of P_2/P_0 moves to smaller distances.

The spectra $P_{1,\omega}$ and $P_{2,\omega}$ for the backward and forward case are shown in Fig. 4 for $d = 2$ μm and 15 μm. It is apparent that for the forward direction $P_{2,\omega}$ is dominated by the high-frequency resonance with magnetic quantum number $m = -1$ of the nanoparticles and for the backward direction $P_{1,\omega}$ is dominated by the low-frequency resonance with magnetic quantum number $m = +1$. Furthermore, it can be observed that for $d = 2$ μm we have $P_2 > P_1$ and for $d = 15$ μm $P_1 > P_2$. Hence, there is a clear rectification of the heat flux which changes its direction when changing from near-field to far-field interparticle distances d. Furthermore, since P_2 (P_1) can only be due to the coupling to the surface waves traveling in positive (negative) x direction, this suggest that the localized particle resonance with $m = +1$ having negative spin couples preferably to the surface wave with negative spin and the particle resonance with $m = -1$ having positive spin to the surface wave with positive spin. Hence, our

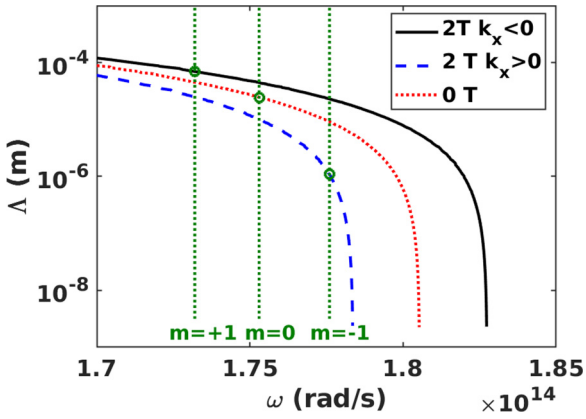

FIG. 5. Propagation length $\Lambda^{\pm}$ of the surface modes for $B = 0$ and 2T. The vertical lines mark the spectral position of the particle resonance with magnetic quantum numbers $m = 0, \pm 1$ for $B = 2$ T. The circles mark the intersection of the particle resonances with the surface mode resonances.

results suggest that there is a selection rule allowing preferred coupling between particle and surface resonances with the same spin.

From this coupling mechanism, we can also understand the position of the maximum in P_1/P_0 and P_2/P_0. To this end, we consider now the propagation length of the surface modes, which is defined as

$$\Lambda^{\pm} = \frac{1}{\pm 2\mathrm{Im}(k_x^{\pm})}, \tag{31}$$

where $k_x^{\pm}$ is the complex solution k_x with $\mathrm{Re}(k_x) > 0$ or $\mathrm{Re}(k_x) < 0$ of the dispersion relation in Eq. (26) for a given real frequency ω. Note that this determines only the propagation length of surface waves with $k_y = 0$. In general, also surface waves with $k_y \neq 0$ which are included in our heat flux calculation have an impact on the heat transfer between the particles. Therefore $\Lambda^{\pm}$ is only a rough estimate of the length scale of the propagation length of the surface waves contributing to the full heat transfer.

In Fig. 5, we show a plot of this propagation length $\Lambda^{\pm}$ for the surface waves traveling in positive and negative x direction for $B = 0$ and 2 T together with the spectral position of the three particle resonances with $m = 0, \pm 1$ for $B = 2$ T. Note that, for $B = 0$ T, all resonances are at the same frequency as the $m = 0$ resonance. In Fig. 5, it can be observed that the propagation length of the surface wave traveling in positive (negative) x direction which couples to the $m = -1$ ($m = +1$) resonance has a much smaller (larger) propagation length of about 1 μm (100 μm) for $B = 2$ T than the 20 μm propagation length for $B = 0$ T. Furthermore, these values of the propagation length are in good agreement with the position d_m of the maxima observed in Fig. 3 explaining why for small distance $P_2 > P_1$ and for large distances $P_1 > P_2$. Hence, from the coupling mechanism, the spectral shift of the particle resonances and the surface mode resonances we can understand the position of the maxima observed in P_1/P_0 and P_2/P_0 as function of the distance. A similar distance dependence has been observed for the positions of the maxima in Förster resonance energy transfer above plasmonic surfaces

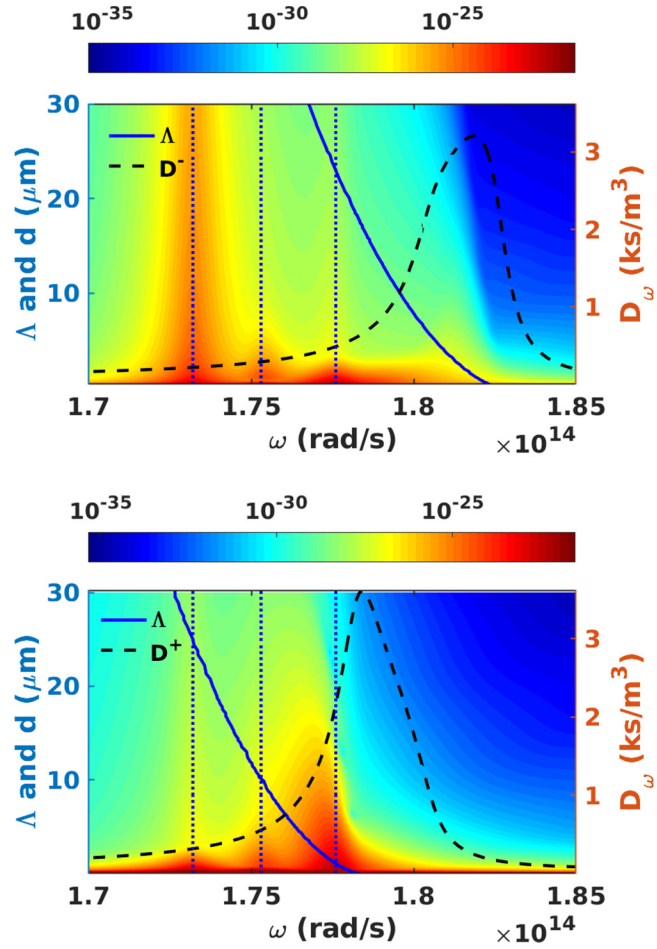

FIG. 6. Spectral net power transfer $P_{1,\omega}$ (top) and $P_{2,\omega}$ (bottom) as function of interparticle distance d and frequency ω for an applied magnetic field of $B = 2$ T and a distance of $z = 5R = 500$ nm to the substrate. Moreover, the propagation length $\Lambda^{\pm}$ and the LDOS $D^{\pm}$ are shown. The dashed vertical lines mark the position of the particle resonance frequencies $\omega_{m=0,\pm 1}$.

[31]. Furthermore, it is clear from Fig. 5 that due to blueshift of the $m = -1$ resonance and the redshift of the surface modes traveling in positive x direction, there can be no coupling anymore for large enough magnetic fields so that for large B one clearly has $P_1 > P_2$ in the surface mode dominated heat transport regime.

To get a more complete picture, in Fig. 6, we show the spectral power $P_{1,\omega}$ and $P_{2,\omega}$ as function of frequency and interparticle distance d together with the position of the three particle resonances, the propagation length $\Lambda^{\pm}$ and the LDOS $D^{\pm}$ from Eqs. (29) and (30). For $d \ll z$, it can be seen that all three resonances contribute to the heat transfer due to the fact that the heat flux is mainly directly transferred between both particles. For larger d, the heat transfer between both particles is more and more dominated by the coupling to the surface modes where the $m = +1$ resonance couples to the long-range surface mode traveling to negative x direction and the $m = -1$ resonance couples to the short range surface mode traveling to the positive x direction. For distances much larger than $\Lambda^{\pm}$, the surface mode contribution vanishes. That $P_2 > P_1$ for small distances d can now also be understood by the fact

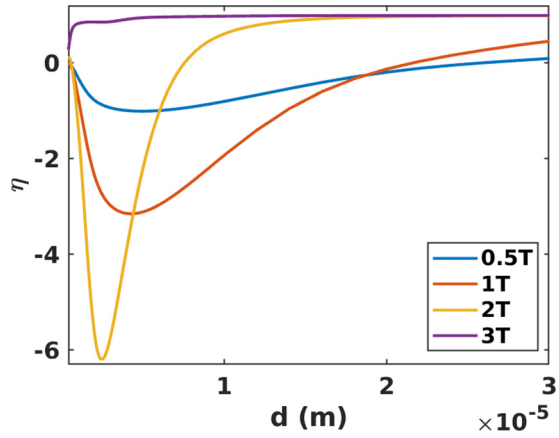

FIG. 7. Rectification coefficient η over the distance d between the particles for different strenghts of the magnetic field $B = 0.5,\ 1,\ 2,$ and 3 T. Again we choose $z = 5R = 500$ nm.

that the LDOS D^+ is larger at $\omega_{m=-1}$ than D^- at $\omega_{m=+1}$. For large distances $d > \Lambda^+$, only the long-range surface modes can contribute and therefore $P_1 > P_2$.

VIII. HEAT FLUX RECTIFICATION

To quantify the heat flux rectification we define the rectification coefficient as [38]

$$\eta = \frac{P_1 - P_2}{P_1}. \tag{32}$$

In Fig. 7, we plot the rectification coefficient as function of d for different magnetic field strengths. It can be observed that for field amplitudes smaller than 3 T the rectification coefficient is negative, because $P_2 > P_1$. For large field amplitudes like $B = 3$ T, the rectification coefficient is purely positive, because $P_1 > P_2$. As discussed before, this is due to the fact that with increasing field strength the resonance $\omega_{m=-1}$ is blue shifted and the surface mode resonance is redshifted leading to a decreasing propagation length Λ^+. This behavior can here be observed in the shift of the position where $\eta = 0$ to smaller distances d when the field amplitude is increased. For $B = 3$ T, the particle resonance $\omega_{m=-1}$ can simply not couple to a surface mode propagating to positive x direction anymore, because the redshift of the particle resonance and the blue shift of the surface mode resonance are too large. Hence, for 3 T, we find $P_1 > P_2$ for all distances. The curves for 2 and 3 T, converge for $d \gg \Lambda^+$ to a rectification coefficient which is close to 1 ($\eta = 0.996$) which means that $P_1 \gg P_2$ which is a clear diode effect. On the other hand, for relatively weak fields and small distances d we have a "minimal" η of about -6 which simply means that $P_2 \approx 7P_1$. If we would in this case define the rectification coefficient as $\tilde{\eta} = (P_2 - P_1)/P_2$ we would obtain $\tilde{\eta} \approx 0.86$. Hence, also in this case we have a large rectification, but in the other direction.

IX. MEAN POYNTING VECTOR

To have a deeper understanding of the heat flow and the spin-spin coupling we determine now the mean Poynting vector $\langle \vec{S} \rangle$ due to the thermal radiation of the two particles in a given environment. As before we provide the general expression for an arbitrary number N of nanoparticles, first, and then invoke the special case $N = 2$. With the electric field

$$\vec{E}(\mathbf{r}) = \omega^2 \mu_0 \sum_{i=0}^{N} \mathbb{G}^{\mathrm{EE}}(\mathbf{r}, \mathbf{r}_i)\vec{p}_i + \vec{E}^b(\mathbf{r}) \tag{33}$$

produced by the thermal background radiation and the thermal dipole moments of the nanoparticles in Eq. (2) we can determine directly the magnetic field by Faraday's law $\vec{H} = \nabla \times \vec{E}/(\mathrm{i}\omega\mu_0)$. Then the mean Poynting vector $\langle \vec{S}_\omega \rangle = 2\mathrm{Re}\langle \vec{E}_\omega \times \vec{H}_\omega \rangle$ can be straight-forwardly determined by using the fluctuation-dissipation theorem of the fluctuational dipole moments in Eq. (9) and of the fields in Eq. (8) and [52]

$$\langle \vec{E}_i^{\mathrm{b}} \otimes \vec{H}_j^{\mathrm{b}} \rangle = 2\omega^2 \mu_0 \hbar \Big(n_b + \frac{1}{2} \Big) \frac{\mathbb{G}_{ij}^{\mathrm{EH}} - \mathbb{G}_{ji}^{\mathrm{HE}\dagger}}{2\mathrm{i}}. \tag{34}$$

We obtain

$$\begin{aligned} \langle S_{\omega,\alpha} \rangle = 4\hbar\omega^2 \mu_0 k_0^2 \sum_{\beta,\gamma=x,y,z} \epsilon_{\alpha\beta\gamma} \mathrm{Re} \\ \times \Bigg[\sum_{i,j,k=1}^{N} (n_j - n_b) \mathbb{G}_{0i}^{\mathrm{EE}} \boldsymbol{T}_{ij}^{-1} \underline{\underline{\chi}}_j \big(\mathbb{G}_{0k}^{\mathrm{HE}} \boldsymbol{T}_{kj}^{-1} \big)^\dagger \\ + \frac{n_b}{2\mathrm{i}} \sum_{i,j=1}^{N} \Big(\mathbb{G}_{0i}^{\mathrm{EE}} \boldsymbol{T}_{ij}^{-1} \underline{\underline{\alpha}} \mathbb{G}_{j0}^{\mathrm{EH}} - \big(\mathbb{G}_{0i}^{\mathrm{HE}} \boldsymbol{T}_{ij}^{-1} \underline{\underline{\alpha}} \mathbb{G}_{j0}^{\mathrm{EE}} \big)^\dagger \Big) \\ + \frac{n_b}{k_0^2} \Big(\frac{\mathbb{G}_{00}^{\mathrm{EH}} - \mathbb{G}_{00}^{\mathrm{HE}\dagger}}{2\mathrm{i}} \Big) \Bigg]_{\beta\gamma}, \end{aligned} \tag{35}$$

where $\epsilon_{\alpha\beta\gamma}$ is the Levi-Civita tensor, $\mathbb{G}_{0i}^{\mathrm{EE}} = \mathbb{G}^{\mathrm{EE}}(\mathbf{r}, \mathbf{r}_i)$ and $\mathbb{G}_{0k}^{\mathrm{HE}} = \mathbb{G}_{0k}^{\mathrm{HE}}(\mathbf{r}, \mathbf{r}_k)$, etc. are the electric and magnetic Green functions of electric and magnetic sources as defined in Ref. [43]. The first term determines the heat transfer between the particles and their environment, the third term describes only the background contribution which is for reciprocal backgrounds zero. This term describes the heat flow in the case that there are no nanoparticles. As shown in Ref. [53] for a nonreciprocal medium this contribution persist even in global equilibrium. This persistent heat flux at an interface has also been observed for a single or several nanoparticles [1,6]. Here, in particular, the nonreciprocal surface modes in the InSb substrate will produce a persistent heat flux in positive or negative x direction described by this third term. Since this term fulfills $\nabla \cdot \langle \vec{S} \rangle = 0$ it does not contribute to the heat transfer between the particles [53]. Finally, the second term is an interference term between the background field and the particles. It describes the change of heat flow of the background field due to the presence of the particles.

Since, the second and third term persists in global equilibrium they describe the persistent heat flux of the interface [53] and the nanoparticles [1,6], but they do not describe any heat transfer between the nanoparticles. Therefore the heat transfer between the particles is fully determined by the first term of

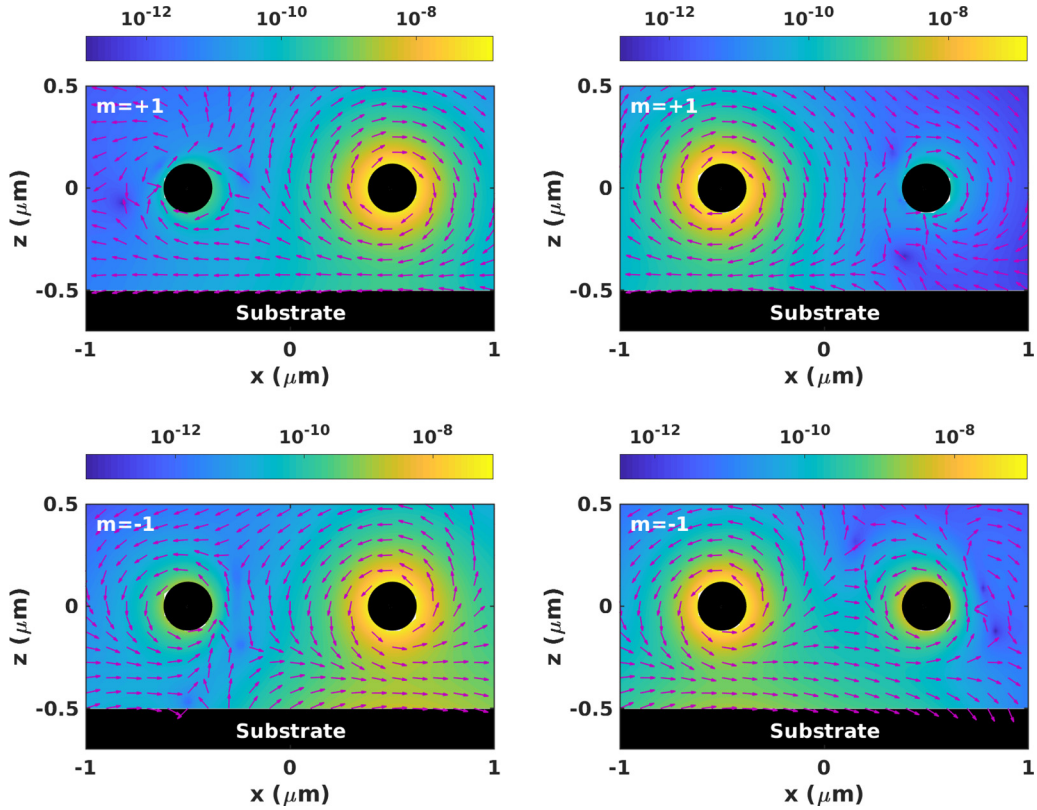

FIG. 8. Spectral in-plane Poynting vector $|\langle S^{\rm tr}_{\omega,x}\rangle\vec{e}_x + \langle S^{\rm tr}_{\omega,z}\rangle\vec{e}_z|$ in (W/m^2) (color scale) and its normalized direction (arrows) for the two InSb nanoparticles (black) with a distance of $z = 5R = 500$ nm to the InSb substrate and interparticle distance $d = 1$ μm for an applied magnetic field of 2T. On the left side, we show the backward case with $T_1 = T_b = 300$K and $T_2 = 350$ K and on the right side the forward case with $T_2 = T_b = 300$ K and $T_1 = 350$ K.

the Poynting vector

$$\left\langle S^{\rm tr}_{\omega,\alpha}\right\rangle = 4\hbar\omega^2\mu_0 k_0^2 \sum_{\beta,\gamma=x,y,z} \epsilon_{\alpha\beta\gamma}\,{\rm Re} \times \left[\sum_{ijk=1}^{N} (n_j - n_b)\mathbb{G}^{\rm EE}_{0i}\boldsymbol{T}^{-1}_{ij}\chi_j(\mathbb{G}^{\rm HE}_{0k}\boldsymbol{T}^{-1}_{kj})^\dagger\right]_{\beta\gamma}. \quad (36)$$

We have checked that for $N = 2$ the integration of the normal component of this Poynting vector on the surface of the nanoparticles 1 and 2 in the backward and forward scenario gives either P_1 or P_2. In Fig. 8, $\langle\vec{S}^{\rm tr}_{\omega}\rangle$ is shown for the different resonance frequencies $\omega_{m=\pm1}$ of the nanoparticles. Again as discussed for a single nanoparticle in Ref. [6] the mean Poynting vector is circulating around the nanoparticles clockwise (counterclockwise) for $m = -1$ ($m = +1$). Moreover, the influence of the substrate can be clearly identified. It can be easily seen that in the forward case the net heat transfer for the $m = +1$ mode is much better then for the $m = -1$ mode and for the backward case it is the other way round. From the counter-clockwise circularity of the $m = -1$ particle resonance it is clear that it couples preferably to surface waves with $k_x < 0$, whereas the clockwise circularity of the $m = +1$ particle resonance clearly suggests a preferred coupling to surface waves with $k_x > 0$. Hence, the mean Poynting vector visualises nicely the spin-spin coupling mechanism of the circular mode in the nanoparticle and the surface modes. Furthermore there seems to be a slight heat flow from the surface towards the nanoparticles for the $m = -1$ resonance in the backward case similar to the heat pumping effect found in Ref. [54].

X. PARTICLE HEATING: WHERE IS THE HEAT GOING?

We have seen that the nonreciprocal surface modes have a strong impact on the heat flux rectification. Furthermore, it could be observed that the heat flux between the nanoparticles is strongly enhanced by the presence of the surface modes as already studied in reciprocal media [22–30]. The evident question is the following: is this enhanced heat flux resulting in an enhanced heating effect? Of course, when bringing the two nanoparticles closer to a substrate they have a new heat flux channel namely the surface modes to exchange heat. On the other hand, they will also radiate more heat into the substrate and one can expect that this effect will be dominant [55]. Therefore, to investigate the diode effect by the nonreciprocal surface waves in more detail, we numerically calculate the particle temperatures in the NESS. We will assume that the temperatures of the hot particle and the background will be fixed to 310 and 300 K in the forward and backward case. The temperature of the cold particle (particle 2 in the forward case and particle 1 in the backward case) which is at $t = 0$ s set to the same value as the background temperature, i.e., 300 K, will be determined by solving the energy balance

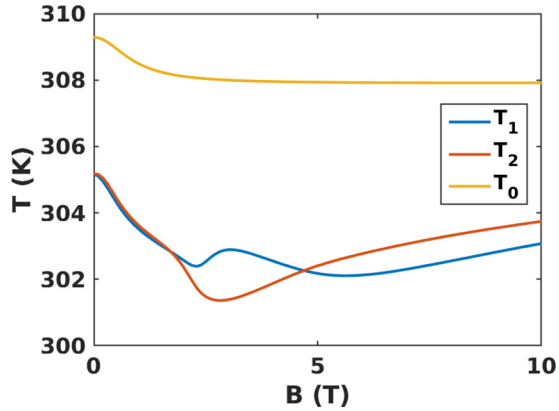

FIG. 9. NESS temperatures of the coulder particle in the forward and backward direction without substrate $T_0 = T_1 = T_2$ and with substrate $T_1 \neq T_2$. We choose $d = z = 5R = 500$ nm.

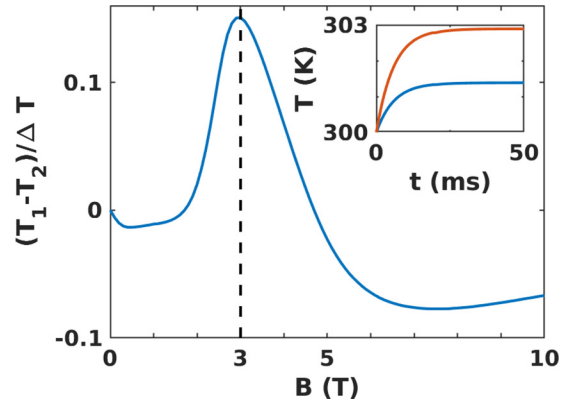

FIG. 10. The temperature difference $(T_1 - T_2)/\Delta T$ for the NESS temperature of the colder particle in backward and forward direction normalized to the initially applied temperature difference of $\Delta T = 10$ K. The inset shows the temperature evolution of T_2 (blue line) and T_1 (red line) in forward and backward case, respectively, from the initial state of 300 K to the NESS for the maximum rectification at 3 T. The distance between the particles and between the particles and the substrate are $d = z = 5R = 500$ nm.

equation [55]

$$\rho C V \frac{dT_k}{dt} = \langle P_k(t, T_1, T_2, T_b) \rangle, \tag{37}$$

for $k = 1$ and 2 with the heat capacity $C = 200\text{J}\,\text{kg}^{-1}\,K^{-1}$, mass density $\rho = 5775$ kg/m^3 and volume V of InSb nanoparticles [56].

In Fig. 9, we show the temperature of the coulder particles in the NESS for the forward and backward case with and without substrate. First, it can be observed that $T_1 = T_2 \equiv T_0$ in forward and backward direction without substrate. Here, the particle temperature of the colder particle is slightly dropping from 309 to 308 K when the magnetic field amplitude is increased. This temperature drop of 1 K (10% of the applied temperature difference $\Delta T = 10$ K) is the giant magnetoresistance effect [3,4]. When the particles are brought in the close vicinity of the substrate at $z = 500$ nm, then the temperature of the colder particle for $B = 0$ T drops from 309 to about 305 K. Hence, a substantial part of the heat emitted by the warmer particle is dissipated in the substrate. Now, when turning on the magnetic field and increasing its amplitude, the temperatures first drop much faster than without surface to about 302 K until $B = 2$T and then for larger amplitudes they rise again up to 303 K/304 K. Hence the surface enhances the giant magnetic resistance effect which is for $B = 2$ T about 30% of the applied temperature difference, i.e., a temperature drop of 3 K.

It can also be seen, that with substrate $T_1 \neq T_2$ in general. In Fig. 10, we show the temperature difference $T_1 - T_2$ of the backward and forward NESS temperatures normalized to $\Delta T = 10$ K. A maximum rectification of about 15% can be observed for relatively large magnetic field amplitudes of $B = 3$ T. For weak fields, the effect is only -1.3%. This is in agreement with the Hall effect, which is also relatively weak for InSb [7]. Hence, a clearly measurable nonreciprocity in the heating can be observed, but due to the fact that most of the heat is going into the substrate, this effect is rather small, but we have not made any optimization. We find that the nonreciprocal heating effect cannot be simply enhanced by for example increasing d or decreasing z. By decreasing z, the surface mode coupling will be stronger, but also the amount of heat going into the substrate. Also decreasing/increasing d is not *a priori* a good option. When decreasing d then the nonreciprocity vanishes due to the fact that for $d \ll z$ the coupling via the surface vanishes. Increasing d on the other hand, will result in large P_1/P_0 and P_2/P_0 as shown in Fig. 3 for $d = 1$ μm, for instance, but the absolute value of the heat flux drops enormously with d so that the heating of the colder particles becomes inefficient. Detailed parameter studies which are out of the scope of our work of the impact of the distance d and z, particles sizes R, and material properties are needed to find optimal materials and configurations to have a strong rectification effect.

XI. CONCLUSION

In summary, we have made a detailed discussion and investigation of the diode working principle of the nonreciprocal near-field diode in Ref. [38]. We have shown that the recitfication effect occurs due to the spin-sensitive coupling of the particle resonances and the surface modes. The transferred heat flux is maximal when the distance between the particle is on the order of the propagation length of the surface modes which is different for the surface modes traveling in positive or negative x direction. Moreover, the strength and direction of the effect is highly dependent on the magnetic field, the distance between the particles and the substrate as well as the local density of states. Our investigation of the mean Poynting vector shows that the spin-sensitive coupling can be understood by the circularity of the particle resonances and the directionality of the surface mode resonances. When the spin of both resonances is the same, these directionalities match explaining the spin-spin coupling. In addition, we find large rectifications of the heat flux with our choice of parameters. Nonetheless, the effective assymmetry in the heating of the nanoparticles in nonequilibrium steady state is for relatively large fields maximally 15% of the initially applied temperature difference between the warm and could nanoparticle.

We believe that the search for optimal parameters and proper materials can lead to a highly increased rectification effect which would make the here discussed concept interesting for future applications.

ACKNOWLEDGMENTS

A. O. and S.-A. B. thank P. Ben-Abdallah, R. Messina, and A. Kittel for helpful discussion and comments. S.-A. B. acknowledges support from Heisenberg Programme of the Deutsche Forschungsgemeinschaft (DFG, German Research Foundation) under the Project No. 404073166.

APPENDIX A: DYADIC GREEN FUNCTIONS

The Green function of the electric field generated by the electric source currents is a sum of the vacuum $\mathbb{G}^0_{ij}$ and the scattered contribution $\mathbb{G}^{\rm sc}_{ij}$ [25]:

$$\mathbb{G}_{ij} = \mathbb{G}^0_{ij} + \mathbb{G}^{\rm sc}_{ij}. \tag{A1}$$

Here, we use the indices i and j to calculate the Green function at position $\vec{r}_i = (x_i, y_i, z_i)^t$ generated by a dipole at position $\vec{r}_j = (x_j, y_j, z_j)^t$.

For the Green function in vacuum, we use [6]

$$\mathbb{G}^0_{ij} = \frac{e^{{\rm i}k_0 d}}{4\pi d}[a\mathbb{1} + b\vec{e}_d \otimes \vec{e}_d] \tag{A2}$$

with $d = |\vec{r}_i - \vec{r}_j|$ and

$$a = 1 + \frac{{\rm i}k_0 d - 1}{k_0^2 d^2}, \tag{A3}$$

$$b = \frac{3 - 3{\rm i}k_0 d - k_0^2 d^2}{k_0^2 d^2}. \tag{A4}$$

The scattered contribution due to the presence of the flat surface is given by

$$\mathbb{G}^{\rm sc}_{ij} = \int_{-\infty}^{\infty}\int_{-\infty}^{\infty} \frac{dk_x dk_y}{(2\pi)^2} e^{{\rm i}(\vec{x}_i - \vec{x}_j)\cdot\vec{\kappa}} \tilde{\mathbb{G}}^{\rm sc}_{ij}(k_x, k_y) \tag{A5}$$

with

$$\tilde{\mathbb{G}}^{\rm sc}_{ij}(k_x, k_y) = \frac{2{\rm i}e^{{\rm i}k_z(z_i + z_j)}}{2k_z} \sum_{k,l=s,p} r_{kl}\vec{a}^+_k \otimes \vec{a}^-_l \tag{A6}$$

using the polarization vectors for s and p polarization

$$\vec{a}^{\pm}_s = \frac{1}{\kappa}\begin{pmatrix} k_x \\ k_y \\ 0 \end{pmatrix} \tag{A7}$$

and

$$\vec{a}^{\pm}_p = \frac{1}{\kappa k_0}\begin{pmatrix} \mp k_z k_x \\ \mp k_z k_y \\ \kappa^2 \end{pmatrix} \tag{A8}$$

with $\vec{x}_i = (x_i, y_i)^t$, $\vec{\kappa} = (k_x, k_y)^t$, and $k_z = \sqrt{k_0^2 - \kappa^2}$. The other Green tensors can be easily calculated from this expression [43].

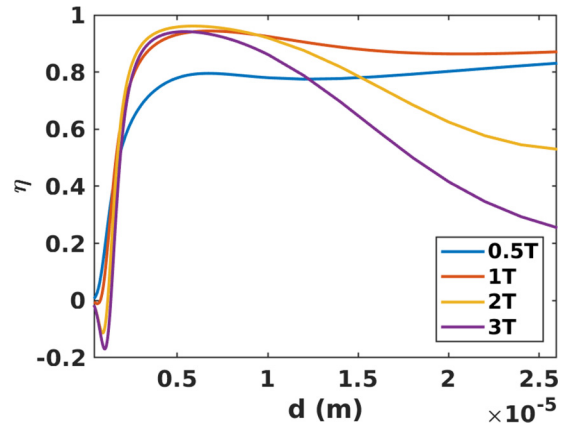

FIG. 11. Rectification coefficient η for a parameter set of InSb as used in Ref. [38] taken from [46] as function of interparticle distance d for different strenghts of the magnetic field and $z = 5R = 500$ nm.

APPENDIX B: IMPACT OF PHONON CONTRIBUTION

The effects discussed in this work highly depend on the material properties. We have chosen throughout the manuscript a parameter set for InSb with a clear dominating electric permittivity. However, for other parameter sets the phononic part may play an important role. Actually, the single surface mode band as seen in the reflection coefficients in Fig. 2 can split into several bands as found in our previous work on the diode effect in Ref. [38], for instance. The discussion given in this work can still be applied to this case, but of course the whole picture becomes more complex.

In order to contrast the impact of the phonons on the rectification coefficient we take now another set of parameters from Ref. [46] with effective mass $m^* = 1.99 \times 10^{-32}$ kg, density of the free charge carriers $n = 1.07 \times 10^{17}$ cm^{-3}, high frequency dielectric constant $\epsilon_\infty = 15.7$, longitudinal and transversal optical phonon frequency $\omega_{\rm L} = 3.62 \times 10^{13}$ rad/s and $\omega_{\rm T} = 3.39 \times 10^{13}$ rad/s. Furthermore, the plasma frequency of the free carriers is $\omega_{\rm p} = \sqrt{\frac{ne^2}{m^*\epsilon_0\epsilon_\infty}} = 3.15 \times 10^{13}$ rad/s. We use further the phonon damping constant $\Gamma = 5.65 \times 10^{11}$ rad/s and the free charge carrier damping constant $\gamma = 3.39 \times 10^{12}$ rad/s. For this set of parameters which we have used in Ref. [38], the rectification coefficient is shown in Fig. 11. In comparison to Fig. 7 it can be seen that in this case the field dependence is much different. In particular, in most cases, $P_1 > P_2$. As could be a priori expected, the rectification effect strongly depends on the doping level of InSb and in particular the directionality. Hence, the rectification effect can be efficiently tailored by changing the doping level. Nonetheless, it should be kept in mind that for nanoparticles also size effects might play a role. For example, for nanoparticles of radius $R = 100$ nm the number of electrons for $n = 1.07 \times 10^{17}$ cm^{-3} is only 450, whereas for $n = 1.36 \times 10^{19}$ cm^{-3} it is 56984, i.e., relatively high. Hence, the optical response of the nanoparticles with a comparably low free charge carrier density like $n = 1.07 \times 10^{17}$ cm^{-3} might be quite different from the bulk response.

[1] L. Zhu and S. Fan, Phys. Rev. Lett. **117**, 134303 (2016).
[2] L. Zhu, Y. Guo, and S. Fan, Phys. Rev. B **97**, 094302 (2018).
[3] I. Latella and P. Ben-Abdallah, Phys. Rev. Lett. **118**, 173902 (2017).
[4] R. M. Abraham Ekeroth, P. Ben-Abdallah, J. C. Cuevas, and A. Garcia Martin, ACS Photon. **5**, 705 (2017).
[5] P. Ben-Abdallah, Phys. Rev. Lett. **116**, 084301 (2016).
[6] A. Ott, P. Ben-Abdallah, and S.-A. Biehs, Phys. Rev. B **97**, 205414 (2018).
[7] A. Ott, R. Messina, P. Ben-Abdallah, and S.-A. Biehs, J. Photon. Energy **9**, 032711 (2019).
[8] E. Moncada-Villa, V. Fernández-Hurtado, F. J. Garcia-Vidal, A. García-Martín, and J. C. Cuevas, Phys. Rev. B **92**, 125418 (2015).
[9] J. Song and Q. Cheng, Phys. Rev. B **94**, 125419 (2016).
[10] H. Wu, Y. Huang, L. Cui, and K. Zhu, Phys. Rev. Appl. **11**, 054020 (2019).
[11] C. R. Otey, W. T. Lau, and S. Fan, Phys. Rev. Lett. **104**, 154301 (2010).
[12] H. Iizuka and S. Fan, J. Appl. Phys. **112**, 024304 (2012).
[13] S. Basu and M. Francoeur, Appl. Phys. Lett. **95**, 231913 (2011).
[14] L. P. Wang and Z. M. Zhang, Nanoscale Microscale Thermophys. Eng. **17**, 337 (2013).
[15] E. Nefzaoui, K. Joulain, J. Drevillon, and Y. Ezzahri, Appl. Phys. Lett. **104**, 103905 (2014).
[16] J. Ordonez-Miranda, K. Joulain, D. De Sousa Meneses, Y. Ezzahri, and J. Drevillon, J. Appl. Phys. **112**, 093105 (2017).
[17] M. M. Qazilbash, M. Brehm, B. G. Chae, P.-C. Ho, G. O. Andreev, B. J. Kim, S. J. Yun, A. V. Balatsky, M. B. Maple, F. Keilmann, H. T. Kim, and D. N. Basov, Science **318**, 1750 (2007).
[18] P. Ben-Abdallah and S.-A. Biehs, Appl. Phys. Lett. **103**, 191907 (2013).
[19] Y. Yang, S. Basu, and L. Wang, Appl. Phys. Lett. **103**, 163101 (2013).
[20] K. Ito, K. Nishikawa, H. Iizuka, and H. Toshiyoshi, Appl. Phys. Lett. **105**, 25350 (2014).
[21] A. Fiorino, D. Thompson, L. Zhu, R. Mittapally, S.-A. Biehs, O. Bezencenet, N. El-Bondry, S. Bansropun, P. Ben-Abdallah, E. Meyhofer, and P. Reddy, ACS Nano **12**, 5774 (2018).
[22] K. Sääskilathi, J. Oksanen, and J. Tulkki, Phys. Rev. B **89**, 134301 (2014).
[23] K. Asheichyk, B. Müller, and M. Krüger, Phys. Rev. B **96**, 155402 (2017).
[24] J. Dong, J. Zhao, and L. Liu, Phys. Rev. B **97**, 075422 (2018).
[25] R. Messina, S.-A. Biehs, and P. Ben-Abdallah, Phys. Rev. B **97**, 165437 (2018).
[26] Y. Zhang, M. Antezza, H.-L. Yi, and H.-P. Tan, Phys. Rev. B **100**, 085426 (2019).
[27] M.-J. He, H. Qi, Y.-T. Ren, Y.-J. Zhao, and M. Antezza, Appl. Phys. Lett. **115**, 263101 (2019)
[28] R. Messina, M. Antezza, and P. Ben-Abdallah, Phys. Rev. Lett. **109**, 244302 (2012).
[29] R. Messina, P. Ben-Abdallah, B. Guizal, M. Antezza, and S.-A. Biehs, Phys. Rev. B **94**, 104301 (2016).
[30] Y. Zhang, H.-L. Yi, H.-P. Tan, and M. Antezza, Phys. Rev. B **100**, 134305 (2019).
[31] S.-A. Biehs and G. S. Agarwal, Appl. Phys. Lett. **103**, 243112 (2013).
[32] S.-A. Biehs, V. M. Menon, and G. S. Agarwal, Phys. Rev. B **93**, 245439 (2016).
[33] R. Deshmukh, S.-A. Biehs, E. Khwaja, T. Galfsky, G. S. Agarwal, and V. M. Menon, ACS Photon. **5**, 2737 (2018).
[34] W. D. Newman, C. L. Cortes, A. Afshar, K. Cadien, A. Meldrum, R. Fedosejevs, and Z. Jacob, Science Adv. **4**, eaar5278 (2018).
[35] J. J. Brion, R. F. Wallis, A. Hartstein, and E. Burstein, Phys. Rev. Lett. **28**, 1455 (1972).
[36] R. Wallis, J. Brion, E. Burstein, and A. Hartstein, Phys. Rev. B **9**, 3424 (1974).
[37] K. Chiu and J. Quinn, Nuovo Cimento B **10**, 1 (1972).
[38] A. Ott, R. Messina, P. Ben-Abdallah, and S.-A. Biehs, Appl. Phys. Lett. **114**, 163105 (2019).
[39] A. Narayanaswamy and G. Chen, Phys. Rev. B **77**, 075125 (2008).
[40] C. Otey and S. Fan, Phys. Rev. B **84**, 245431 (2011).
[41] D. Becerril and C. Noguez, Phys. Rev. B **99**, 045418 (2019).
[42] R. Messina, M. Tschikin, S.-A. Biehs, and P. Ben-Abdallah, Phys. Rev. B **88**, 104307 (2013).
[43] W. Eckhardt, Phys. Rev. A **29**, 1991 (1984).
[44] F. Herz and S.-A. Biehs, Europhys. Lett. **127**, 4 (2019).
[45] S. Law, R. Liu, and D. Wasserman, J. Vac. Sci. Technol. B **32**, 052601 (2014).
[46] E. D. Palik, R. Kaplan, R. W. Gammon, H. Kaplan, R. F. Wallis, and J. J. Quinn, Phys. Rev. B **13**, 2497 (1976)
[47] A. Lakhtakia, V. K. Varadan, and V. V. Varadan, International J. Infrarared and Millimeter Waves **12**, 1253 (1991).
[48] H. C. Chen, Radio Sci. **16**, 1213 (1981).
[49] T. Van Mechelen and Z. Jacob, Optica **3**, 118 (2016).
[50] C. Khandekar and Z. Jacob, New J. Phys. **21**, 103030 (2019).
[51] K. Joulain, R. Carminati, J.-P. Mulet, and J.-J. Greffet, Phys. Rev. B **68**, 245405 (2003).
[52] G. S. Agarwal, Phys. Rev. A **11**, 230 (1975).
[53] M. G. Silveirinha, Phys. Rev. B **95**, 115103 (2017).
[54] P. Ben-Abdallah, Phys. Rev. Lett. **123**, 264301 (2019).
[55] M. Tschikin and S.-A. Biehs and P. Ben-Abdallah and F. S. S. Rosa, Eur. Phys. J. B **85**, 233 (2012).
[56] U. Piesbergen, Z. Naturforschung **18**, 141 (1963).